Correspondence between microwave and submillimeter absorptivity in epitaxial thin films of $YBa_2Cu_3O_7$

D. Miller and P. L. Richards
Department of Physics, University of California, and Materials Sciences Division, Lawrence Berkeley Laboratory, Berkeley, California 94720

S. Etemad, A. Inam, T. Venkatesan, B. Dutta, and X. D. Wu
Bell Communications Research, Red Bank, New Jersey 07701

C. B. Eom and T. H. Geballe
Department of Applied Physics, Stanford University, Stanford California 94305

N. Newman and B. F. Cole
Conductus, Inc., Sunnyvale, California 94086

(Received 12 November 1991; revised manuscript received 4 May 1992)

We have measured the low-temperature loss in six epitaxial *ab*-plane films of the high-T_c superconductor $YBa_2Cu_3O_7$ over a factor of 2000 in frequency. Submillimeter measurements from 25 to 700 cm^{-1} were made at 2 K by a direct absorption technique in which the film acts as the absorbing element in a composite bolometric detector. Microwave measurements near 10 GHz (0.3 cm^{-1}) were made on five of the same films by resonance techniques at 4 K. The $\sim$0.4-μm-thick films were grown epitaxially on $SrTiO_3$, $LaAlO_3$, and MgO by off-axis sputtering and laser deposition. The absorptivities measured for all films studied are qualitatively similar, increasing smoothly with frequency, with no gaplike features below the well-known absorption edge at 450 cm^{-1}. A successful three-parameter fit is obtained for all of our films. This fit can be interpreted either in terms of a weakly coupled grain model or a homogeneous two-fluid model with residual normal conductivity. The fitting parameters correspond to a grain-penetration depth λ_g equal to the muon-spin-relaxation value of 140 nm, and to reasonable grain properties. They also give carrier densities in reasonable agreement with optically determined plasma frequencies and conductivities in agreement with a Kramers-Kronig analysis of the absorptivity data.

I. INTRODUCTION

A knowledge of the loss at microwave, millimeter, and submillimeter frequencies plays an important role in our understanding of the superconducting state properties of high-T_c superconductors such as $YBa_2Cu_3O_7$. These measurements, however, are complicated by several factors, including the anisotropy and complex microstructure of these materials. Advances in the technology of materials fabrication have resulted in the ability to study highly oriented samples. In addition, the sample quality has improved and along with it the reproducibility of the resulting optical spectra. However, the interpretation of such measurements remains somewhat controversial. This is due in part to the lack of a consistent picture of the loss spectrum between microwave and submillimeter frequencies.

One of the most studied cuprate superconductors is the $T_c \sim 90$ K material $YBa_2Cu_3O_7$ (YBCO). Almost all submillimeter measurements of *ab*-plane-oriented YBCO observe an onset of absorption at $\sim$450 cm^{-1}.[1-8] While the amplitude of this absorption feature is strongly temperature dependent near T_c, the characteristic frequency is only weakly temperature dependent even in the neighborhood of T_c.[4] In addition, this feature is present at temperatures both above and below T_c (Ref. 3) in oxygen-deficient samples of this material with low T_c's. Within experimental uncertainties, the onset frequency of this feature is independent of the T_c of the sample.[3] These observations suggest that this feature is not a conventional superconducting energy gap. Another feature commonly observed in reflectivity measurements of *ab*-plane-oriented YBCO is an onset of absorption near 140 cm^{-1} for $T \ll T_c$. Below this frequency the measured reflectivity is observed to be consistent with unity.[2-4,7,9] However, the amplitude of this onset is comparable to the amplitude of the experimental uncertainties in these measurements, which are typically $\pm 1\%$.

Measurements with polarized infrared radiation on untwinned YBCO crystals[10,11] show that the absorption is anisotropic in the *ab*-plane. For current flow perpendicular to the Cu-O chains, the absorption below 500 cm^{-1} is much smaller than for current flow along the chains.

Recently, several groups have measured the transmittance of thin YBCO films[12,13] in order to obtain more accurate data, especially at frequencies below a few hundred wave numbers. Despite the complications associated with the optical properties of the substrate, these experiments suggests that there is some nonvanishing fraction of normal (absorbing) carriers well below T_c. No onset of absorption is observed in these experiments below

450 cm^{-1}.[12]

Three basic interpretations have been given to the infrared data. Some workers have interpreted the frequency at which the measured reflectivity becomes consistent with unity (~ 140 cm^{-1}) with a superconducting gap.[2-4,7,14,15] For the samples with $T_c = 90$ K, this leads to a value for the gap of $2\Delta \approx 2.2 k_B T_c$. Others identify the 450-cm^{-1} feature with the gap,[4,7] giving $2\Delta \approx 7 k_B T_c$ for samples with $T_c = 90$ K. Still others attribute the 450-cm^{-1} feature to a strong electron-phonon interaction[16] and suggest that the relaxation time is short enough in YBCO that no infrared gap should be visible.[2]

Microwave measurements show a temperature-dependent component to the loss which is in reasonable agreement with the predictions of Mattis and Bardeen[17] for temperatures near T_c, e.g., $T > 80$ K, plus a substantial residual loss that remains at low temperatures. This residual loss is minimized in high-quality epitaxial *ab*-plane films. Both contributions to the loss vary as frequency squared from ~ 10 to ~ 100 GHz.[18]

In this paper we present an experimental approach that is used to obtain accurate direct absorptivity data on epitaxial *ab*-plane films in the frequency range between microwave loss and infrared reflectivity measurements.[19] Data are presented for six well-oriented films, four of which are of high quality and are fully oxygenated. Optical measurements of the absorptivity or reflectivity, in principle, give equivalent information for optically thick samples. However, experimentally there is a significant advantage of a direct absorptivity measurement over reflectivity measurements when the sample reflectivities being studied are close to unity, as occurs for these materials below approximately 300 cm^{-1}. Sources of error which tend to multiply the resulting spectra (e.g., drift, sample placement errors, standing waves) which can dominate the signal for reflectivity measurements are minimized in the absorptivity measurement. In addition, uncertainties associated with the precise determination of unity reflectivity are minimized by measuring the absorptivity directly. Also, direct absorptivity measurements are less sensitive to substrate properties than transmissivity measurements. Since the first results of our experiment were announced,[20] similar techniques have been used by others to measure absorptivity in single crystals of YBCO.[21]

Along with the submillimeter absorptivity data, we present microwave surface-resistance measurements made near 10 GHz (0.3 cm^{-1}) and 4 K for five of the six films. Using the well-documented frequency-squared dependence of the microwave loss up to 100 GHz,[18] we can infer the loss in our films over four decades in frequency. The absorptivity varies as frequency squared up to ~ 10 cm^{-1} (300 GHz) and then approaches a constant by 450 cm^{-1}, where there is a sharp onset of additional absorption. We do not observe any absorption onset at 140 cm^{-1} for any of our samples. Other investigators have explored the relationship between the residual microwave loss and the submillimeter absorptivity deduced from reflectivity measurements. Our data are generally consistent with early work,[22] but not with a recent paper which shows higher microwave losses relative to the infrared loss than we observe.[6]

A successful three-parameter fit is obtained for all of our films. This fit can be interpreted either in terms of a weakly coupled grain model or a homogeneous two-fluid model with residual normal conductivity. The fitting parameters correspond to a grain-penetration depth λ_g equal to the muon-spin-relaxation value of 140 nm and to reasonable grain properties. They give carrier densities in agreement with optically determined plasma frequencies and conductivities in agreement with a Kramers-Kronig analysis of the absorptivity data. We use these models to phenomenologically describe the microwave and submillimeter losses in our samples below the absorption onset at 450 cm^{-1}. We do not expect these simple models to describe the absorptivity above the 450-cm^{-1} feature. Since these models are strictly valid only at frequencies below the superconducting gap, our model fitting implicitly assumes that the superconducting energy gap 2Δ, if one exists, occurs at or above 450 cm^{-1}. This analysis is consistent with the results of other workers[2-7] above ~ 400 cm^{-1}. Below ~ 400 cm^{-1}, where our new data play an important role, the results of this analysis are in excellent agreement with the weakly coupled grain-model fitting described above for all films, but not with the conductivity deduced from the two-fluid model.

II. EXPERIMENTAL APPROACH

In order to make a direct measurement of the absorptivity, we have used the high-T_c film as the absorbing element in a composite bolometric far-infrared detector.[23] The 250–500-μm-thick substrates are suspended in a thermal vacuum by 100-μm-thick nylon threads. Typical substrates are 5×5 mm^2. The back surface of each substrate is coated with a gold film to reduce absorption of stray radiation and a small neutron-transmutation-doped (NTD) germanium thermistor[24] and NiCr heater[25] are glued to this surface. The ~ 100-ms thermal time constant $\tau = C/G$ of the bolometer is determined by the heat capacity C of the assembled bolometer and the thermal conductance G due to the electrical leads from the thermistor to the heat sink at ~ 1.5 K.

A schematic of the experimental apparatus is shown in Fig. 1. Infrared radiation (A) chopped at 10 Hz from a Fourier-transform spectrometer operated in the step-and-integrate mode passes through a light pipe and a cold low-pass filter to a roof mirror (B) which divides the beam symmetrically between the sample bolometer (I) and a reference bolometer with known absorptivity (II). The aperture (C) of a thin-walled brass tube (not shown), which is pressed against the absorbing film, defines the throughput $A\Omega \approx 0.03$ sr cm^2 onto each film. The absorbing film is located on the front surface of the substrate (E), which is held firmly against the exit of the throughput limiter by tension in the nylon threads (F), which are suspended from a support ring (G). The absorbing films are electrically isolated from the throughput limiters and are surrounded by infrared absorber[26] (D) to reduce stray radiation. The support ring (G) also serves as a heat sink (L) for the electrical connections (H) to the

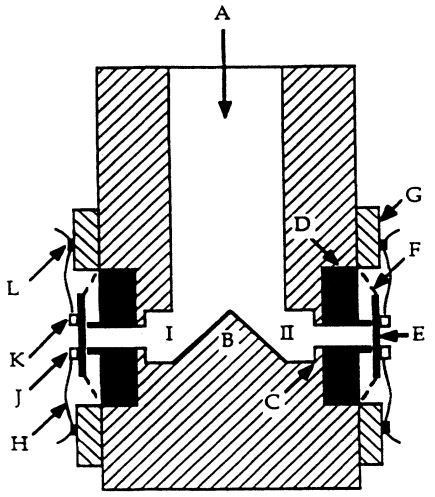

FIG. 1. Cross section of the apparatus, which is operated in a thermal vacuum at ~1.5 K. Incident radiation A is split by roof mirror B and sent to detector channels I and II. In each channel a throughput limiter C defines the incident radiation. Stray radiation is absorbed by baffles D. The film being measured is located on the front inner surface of a substrate E, which is suspended by nylon threads F from the support ring G. Thermistors J and resistance heaters K are indicated schematically. Electrical connections H to thermistors and resistors provided the thermal conductance between the substrate and the heat sinks L.

thermistor (J) and heater resistor (K). Frequency-dependent asymmetries in the throughput are measured and corrected by interchanging sample and reference detectors.

The frequency dependence of the response to an ac current through the heater and to chopped infrared radiation are measured to confirm that all internal thermal relaxation times in the bolometer are much shorter than C/G. Under these conditions the responsivity R^f of the bolometer to absorbed infrared power at frequency f can be measured by passing an ac current at frequency $f/2$ through the known heater resistance.

The output spectrum from each detector channel can be represented by $F(\omega)=L(\omega)A(\omega)R^f$, where ω is the frequency, $L(\omega)$ is the submillimeter spectrum incident on the absorbing film from the spectrometer, $A(\omega)$ is the absorptivity of the film, and R^f is the responsivity of the detector to absorbed power. If the detector responsivities and the absorptivity of the reference detector are known, then the absorptivity of the sample can be determined from

$$A_s(\omega)=\frac{F_s(\omega)R_r^f}{F_r(\omega)R_s^f}A_r(\omega)\ , \tag{1}$$

where the subscripts s and r refer to the sample and reference channels, respectively, and where $A_r(\omega)$ is the known absorptivity of the reference absorber.

The success of this experiment depends on the availability of a reference film with known absorptivity. In addition, the reference absorber should have a small heat capacity and an absorptivity comparable to that of the sample. For this reason we use a sputtered gold film. No special precautions are taken to ensure the purity of the sputtered metal, and so the conductivity of the film is low enough that the absorptivity can be calculated from classical skin-effect theory using the conductivity $\sigma(\omega)=\sigma_{dc}/(1-i\omega\tau)$. Here $\sigma_{dc}=ne^2\tau/m$ is the dc conductivity of the gold film measured at 4 K and τ is the momentum relaxation time inferred from σ_{dc} assuming a free-electron mass and a carrier density of one electron per atom.[27]

Because of surface imperfections, the optical absorptivity calculated from the bulk dc properties will underestimate the actual film absorptivity.[28] In order to correct for this effect, we have measured the absorptivity of an etched brass foil relative to the gold reference. By fitting the ratio of absorptivities of brass and gold to a Drude model for each of the materials, we are able to determine an effective dc conductivity and carrier density for both the brass and gold. The use of these effective parameters should then partially compensate for the effects of surface imperfections.

The absorptivity of the brass is calculated from classical skin-effect theory using the dc conductivity of the brass measured at 4 K and the carrier density estimated from a room-temperature Hall-coefficient measurement[29] assuming a single-carrier band. We calculate the ratio of the absorptivities of brass and gold from the respective dc material properties and also from a best fit to the measured infrared ratio. The measured infrared ratio and the absorptivity ratio determined from the dc properties of the brass and gold, as well as the best-fit absorptivity ratio, are shown in Fig. 2. A list of the dc and best-fit parameters for the brass and gold is given in Table I.

The agreement between the directly measured ratio and the ratio determined from the dc properties is quite good between 30 and 650 cm^{-1}; the agreement between the directly measured ratio and the best fit is excellent over the same frequency range. Because the optical data accounts more accurately for the actual surface properties of the gold film than the simple theory, we use the ab-

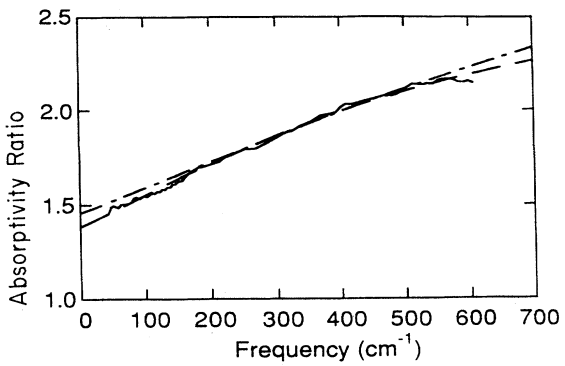

FIG. 2. Ratio of the measured absorptivity of brass and gold, as described in text. The solid line is the experimental data. The dashed line is the best fit of the Drude model to the data. The dot-dashed line is the fit of the Drude model using the measured dc properties of the brass and gold.

TABLE I. Parameters used in the Drude model for determining the absorptivities of Au and brass.

	Carrier density n (10^{22} cm^{-3})		Electrical resistivity ρ ($\mu\Omega$ cm)	
	dc	Best fit	dc	Best fit
Au	5.9	3.6	5.5	5.9
Brass	19.0	7.4	11.6	11.3

sorptivity of the gold film determined from the best fit of the optical data to characterize the gold film. The correction to the frequency-dependent absorptivity of the gold film varies smoothly with frequency. At 30 (700) cm^{-1}, the best-fit absorptivity is 3% higher (15% lower) than the absorptivity determined from the dc properties of the gold alone.

Deviations between the best fit and the absorptivity ratio in Fig. 2 help to establish the valid range of the optical data. The reproducibility of the data is poor above 650 cm^{-1}. This may reflect the sensitivity of the spectrometer to thermal drifts at these high frequencies. Deviations are seen below 30 cm^{-1} which appear to be due to the decreasing effectiveness of the light baffles surrounding the sample. The light baffles become transparent below $\sim$30 cm^{-1}.[30] This effect leads to an overestimation of $A(\omega)$. Because the sample and reference absorptivities are not identical, this error does not cancel out when the ratio of absorptivities is calculated.

As a test of the method, we have measured the absorptivity of a 250-nm Nb film at 2 K, which is shown in Fig. 3. Note that we are able to observe a superconducting gap in the Nb film at $\sim$25 cm^{-1}, where the absorptivity is less than 0.5%.

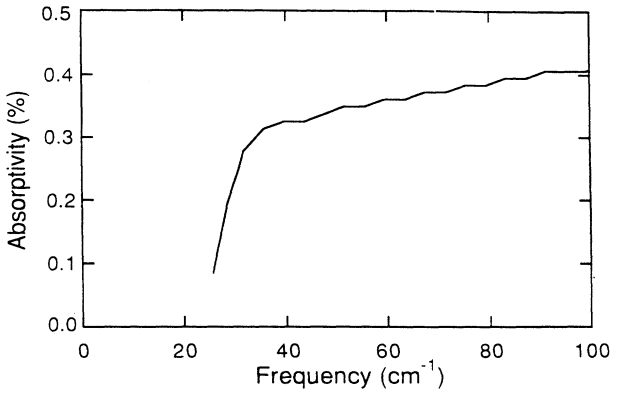

FIG. 3. Measured absorptivity of Nb thin film at 2 K. The residual resistivity ratio for this film is $\sim$6–7, and the microwave loss is nominally 20 $\mu\Omega$ at 4 K and 10 GHz.

III. SAMPLE CHARACTERIZATION

The samples used in this study were fabricated by three different research groups using two different techniques and were grown on MgO,[31] $LaAlO_3$,[32,33] and $SrTiO_3$ (Refs. 33 and 34) substrates. A list of the samples studied is found in Table II. Samples A, B, C, and E were fabricated with a 90° off-axis sputtering technique from a composite YBCO target.[31,32] Substrates were attached to a substrate block heated to approximately 700° C with either a mechanical clamp or silver paste or both. Approximately 100 W of power on the sputter gun gave a deposition rate for the off-axis geometry of less than 0.1 Å/s, depending on the sputtering atmosphere, which varied between 10–100 mTorr O_2 (or N_2O) and 40–300 mTorr Ar. Samples D and F were fabricated with a laser deposition technique using a 248-nm KrF excimer laser fired at 1 Hz onto a rotating composite YBCO target.[33,34] The plume of ejected materials was collected onto substrates which were heated to approximately 700 °C, with typical deposition rates of 1 Å/s. A jet of oxygen was directed toward the center of the plume, while the background pressure was maintained at approximately 10 mTorr.

The samples used in this study are notable for their lack of impurity phase and high degree of epitaxial alignment perpendicular to their surface, with the YBCO c axis perpendicular to the substrate surface. Compositional analysis with Rutherford-backscattering spectrometry indicated that the films used in this study were in the 1:2:3 phase.[32,35,36] Crystalline quality was studied by measuring x-ray rocking-curve widths for films nominally identical to those used in this study[31,34,35,37,38] and suggest within the limitations of the experiment that these films have nearly perfect single-crystalline structure. However, transmission and scanning electron microscopy studies indicate that these films are heavily faulted. This apparent contradiction between x-ray and electron stud-

TABLE II. Samples measured in this work. Values of microwave surface resistance R_s measured at 4 K near 10 GHz are scaled to 10 GHz using an ω^2 law, where ω is the microwave frequency. Superconducting transition temperatures are measured from midpoint of transition; transition widths are measured from 10–90% of transition. Approximate values for the dc resistivity ρ_n measured at 300 K are listed for comparison.

Sample	Institution	Thickness (nm)	Substrate	$T_c/\delta T$ (K)	Deposition technique	R_s ($\mu\Omega$)	ρ_n (300 K) ($\mu\Omega$ cm)
A	Stanford	500	MgO	85/1.0	off-axis sputter	12	195
B	Stanford	400	MgO	85/1.0	off-axis sputter	16	260
C	Conductus	410	$LaAlO_3$	87/1.0	off-axis sputter	30	330
D	Bellcore	500	$LaAlO_3$	92/0.5	laser ablation	48	
E	Conductus	1250	$LaAlO_3$	87/2.0	off-axis sputter	180	600
F	Bellcore	480	$SrTiO_3$	89/0.5	laser ablation		200

ies can be resolved by recalling that x rays are less sensitive to small-scale structure than electrons, which have shorter wavelengths and coherence lengths.[34]

The microstructure of the laser-deposited films on $LaAlO_3$ and $SrTiO_3$ exhibit undulations both along the (001) planes (*c* layers) and the (110) planes, with a typical structural correlation range of about 10 nm.[34] These films are nevertheless free from macroscopic grain boundaries[2,34,35] and are very homogeneous, with surface roughness less than 15 nm, and are free from any secondary phase. In contrast, laser-deposited films on MgO, or films deposited onto $LaAlO_3$ or $SrTiO_3$ substrates heated above 700 °C, contain grain boundaries of a few μm or larger.[34,39] Typical *c*-axis-oriented films deposited by off-axis sputtering exhibit a high density of intersecting (110) twins, with typical spacings ranging from 10 to 70 nm and with twin lengths from 20 to 200 nm.[36] Typical surface roughness for *c*-axis films deposited onto MgO is less than 5 nm.[36] Films deposited on $LaAlO_3$ can be rougher.[38] In addition, the off-axis sputtered films contain a small volume fraction of *a*-axis-oriented grains,[36,38] typically less than 1%.

In-plane film texture was examined by studying x-ray ϕ scans.[40] Both $LaAlO_3$ and $SrTiO_3$ and the 1:2:3 phase of YBCO have a perovskite structure, and the lattice match between these materials is good. However, a 7–9 % lattice mismatch for MgO and YBCO in the (001) crystallographic direction may, under nonoptimal growth conditions, lead to the formation of grains in which the in-plane unit-cell axis of the film is aligned with the (110) axis of the substrate, corresponding to a rotation of 45°. The size of these 45°-rotated domains ranges from 0.5 to 10.0 μm.[36] Off-axis sputtered films on MgO typically contain less than 1% volume fraction of such misoriented grains and misorientations of other distinct angles.[36]

A positive correlation has been found by others between the volume fraction of high-angle (45°) grain boundaries and R_s for YBCO films on MgO.[37] However, other studies of YBCO thin films on $LaAlO_3$ have found a lack of correlation between R_s and structural properties such as the quantity of 45°-misoriented material. In fact, film E on $LaAlO_3$, with a fairly large $R_s = 180$ $\mu\Omega$, was found to have a very small (0.06%) volume fraction of 45°-misoriented material.[32]

IV. MICROWAVE MEASUREMENTS

The microwave surface resistance R_s of samples A, B, C, and E was measured at 11–13 GHz with a parallel-plate resonator technique, described elsewhere.[41] Two flat superconducting films of the same nominal area with a thin dielectric spacer between them form the resonator. By using a dielectric spacer with a small loss tangent and making the spacer as thin as possible, it is found that the Q of the resonator is dominated by the loss in the superconducting film and is therefore inversely proportional to the surface resistance of the film. In this analysis it is assumed that the films are thick enough that rf power is not transmitted through the film. If the films are too thin, then the measured value of the surface resistance will be lower than for a thick film of similar material. Values of R_s quoted for the films measured with this technique do not include any correction for radiation loss.[32,37,38,41] The effects of the finite film thickness on these measurements is discussed below.

The surface resistance of sample D was measured by placing it in a superconducting niobium cavity operated in the TE_{011} mode at 5.95 GHz as described elsewhere.[42] The value of cavity Q was converted into surface resistance by comparison with the measured Q and the calculated surface resistance of a Nb foil with nominally the same area as the sample. In this measurement rf currents are induced in both the upper and lower surfaces of the film. The substrate losses are subtracted from the result through a separate measurement of a bare substrate. The resulting value of R_s is an average for the two surfaces and may contain contributions from losses at the interface between the film and substrate.

The effect of the finite film thickness on the measurement of the microwave surface resistance has been examined by Klein *et al.*[43] at 87 GHz and 77 K by treating the film-substrate system as a transmission line and approximating the surface impedance of a hypothetical thick slab of superconductor as $Z_\infty = R_\infty - i4\pi\omega\lambda/c^2$, where R_∞ and Z_∞ correspond to the surface resistance and complex impedance, respectively, of the hypothetical thick slab. This treatment is a useful guide to the effects of the finite film thickness on observed surface impedance. The concept of a bulk impedance Z_∞ is of limited validity for high-T_c films, however, since the microstructure of these materials, and hence Z_∞, can depend in a complicated way on sample thickness.[36,41]

We have done similar calculations at 10 GHz and 4 K using $\lambda = 140$ nm and treating the sample as a thin superconducting film of bulk impedance Z_∞ on a 500-μm substrate of $LaAlO_3$ backed by free space. We find that measured surface impedances at 10 GHz and 4 K can depend on film thickness for films thinner than $\sim$500 nm. For films thicker than 300 nm, however, we find that R_∞ will be at most 25% lower than the measured R_s for films with measured $R_s > 10$ $\mu\Omega$. We have done similar calculations at 1 THz, corresponding to the lowest frequencies of the submillimeter absorptivity measurement, and find that no correction to the measured absorptivity is required for the range of measured absorptivities and film thicknesses studied.

V. RESULTS

Absorptivity data for sample F are plotted in Fig. 4 along with $1-R(\omega)$, where $R(\omega)$ is the reflectivity reported earlier on the sample.[2] Certain features, such as the small knee just below 500 cm^{-1} and the plateau between 200 and 400 cm^{-1}, exist in both data sets, but there are differences in the overall level and slope. The two data sets can be brought into very good agreement if we plot $0.85[1-R(\omega)]+1.1\%$. The additive constant may reflect the uncertainty associated with knowing the precise signal level corresponding to unity reflectivity in the reflectivity measurement. The reason for the discrepancy in slope is not known.

In order to test whether the discrepancy in Fig. 4 could

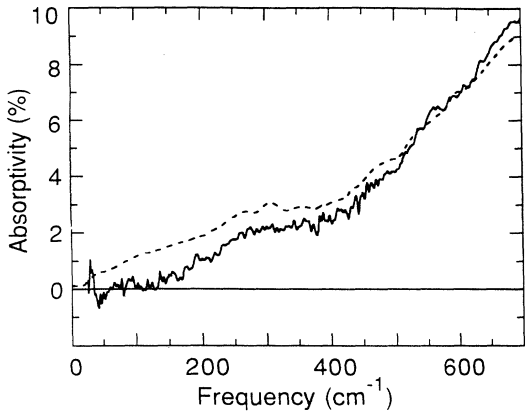

FIG. 4. Absorptivity of sample F measured directly at 2 K by the technique described in this work (dashed line) and deduced from a reflectivity measurement made at Bellcore at 15 K (solid line).

be due to the loss of oxygen from the film in the 3 months between the reflectivity and absorptivity measurements, the absorptivities of this and several other films were measured before and after both plasma oxygenation and ion bombardment. Ratios of spectra measured before and after treatment showed observable differences which were fractionally more important in the low-frequency part of our range, but neither the sign of the effect nor the frequency dependence was reproducible.

Absorptivity data for samples A–E are plotted in Fig. 5. The absorptivities for all samples are nonvanishing down to the lowest frequencies measured. Despite the varying deposition techniques and substrates, the infrared absorptivity spectra for samples A–D are qualitatively similar. This indicates that although we may not be observing the intrinsic absorptivity of the YBCO, we are at least observing a reproducible optical signature which is insensitive to the detailed sample characteristics of high-quality films. For these films the absorptivity is approximately monotonic. It increases from the lowest frequencies up to 300 cm^{-1} and has a plateau from ~300 to 450 cm^{-1}, above which there is an onset of additional absorptivity. There is no sign of any gap-like onset of absorption either near the BCS value of $3.5k_BT_c \approx 220$ cm^{-1} or near 140 cm^{-1}.[2–4,7,9] We observe distinct optical features in sample E at 150 and 310 cm^{-1} which are weakly present in sample A at 150 cm^{-1} and in all films measured at 310 cm^{-1}. These features have been identified as infrared-active lattice modes.[44] Because of screening by the high conductivity in the *ab* plane, observation of phonon modes is expected only for electric-field excitations along the *c* axis. Both the appearance of these modes and the higher overall absorptivity show that samples C and E are of significantly lower quality than samples A, B, and D. (Sample E was intentionally sputtered in an O_2-deficient atmosphere in order to have higher loss than the other films.)

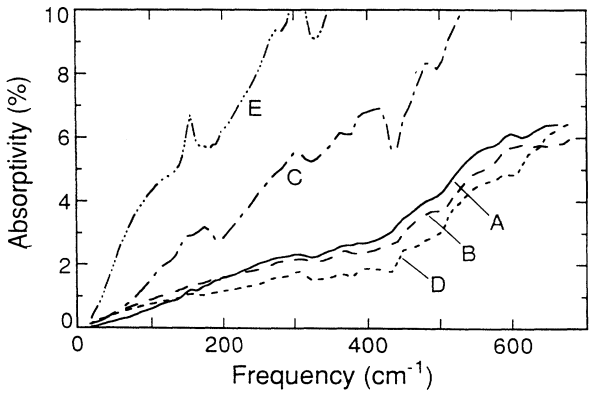

FIG. 5. Measured absorptivity of samples A–E at 2 K. Sample E was intentionally prepared to give a large microwave loss.

Because of the low critical field H_{c1} for these superconductors, it is certain that there is trapped flux in thin films at low temperatures due to the laboratory magnetic field. Flux motion driven by the incident radiation is a potential source of the loss. In order to explore this effect, fields of approximately 10 G were applied normal to the films with both the smallest and largest microwave R_s. No significant differences in the measured absorptivities were observed.

VI. DATA ANALYSIS

A. Introduction

Absorptivity data for samples A–E are again plotted in Fig. 6 along with two theoretical fits described below.

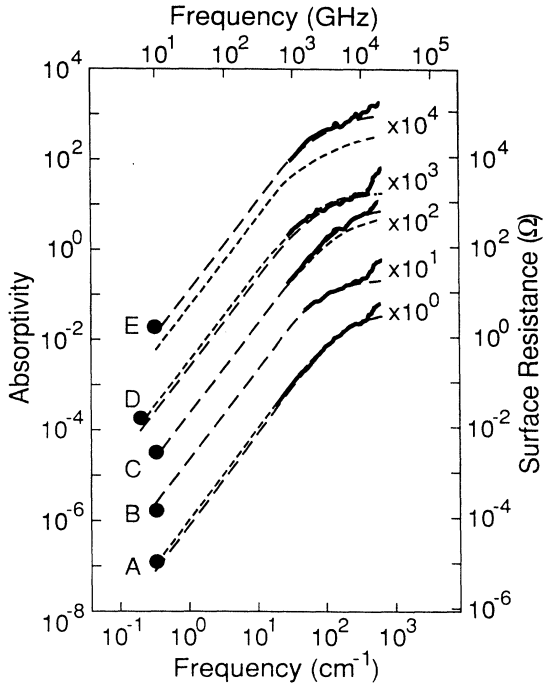

FIG. 6. Measured submillimeter absorptivities of samples A–E at 2 K (solid lines) multiplied by the indicated factors to separate the curves. Values of the microwave surface resistance measured for each sample at 4 K are shown as solid circles. Also shown are two different fits to the absorptivity data. The interpretation of the long-dashed lines (fit I) and the short-dashed lines (fit II) is given in the text in terms of the weakly coupled grain and two-fluid models.

This logarithmic plot emphasizes the low-frequency range of the submillimeter measurement and allows a comparison with the microwave measurements made on the same samples. The curves in this plot are displaced by factors of 10 to avoid overlap. The microwave-loss measurements at 4 K are indicated by the solid circles for each film. The size of the circles is large enough to include estimated errors and corrections for film transparency. The solid lines give the submillimeter absorptivity measurements at 2 K. Additive errors are thought to be small down to the lowest frequencies presented. Multiplicative errors could be as large as 15% (see Sec. II). These results give a picture of the residual loss in epitaxial *ab*-plane YBCO films over nearly four decades in frequency. For each film, the 10-GHz point can be connected to the submillimeter data at ~ 30 cm^{-1} by a line which varies as frequency squared. This agrees with Piel and Muller[18] in the range from 10 to ~ 100 GHZ (0.3–30 cm^{-1}), but is in disagreement with Renk *et al.*,[6] who observe the loss to be linear in frequency between 87 GHz (~ 3 cm^{-1}) and 30 cm^{-1}. The frequency dependence of the loss saturates smoothly above 30 cm^{-1} in a way that is different for different films. In contrast to the results of Pham *et al.*[21] on single crystals, we do not observe the loss to vary quadratically with frequency in the range from 100 to 400 cm^{-1}.

We have analyzed data for films A–E in terms of a homogeneous two-fluid model and in terms of a model proposed by Hylton *et al.*[45,46] that treats polycrystalline high-T_c films as a network of weakly coupled grains. We have also used the Kramers-Kronig (KK) transform method to calculate the complex conductivity $\sigma(\omega)$ from the loss data for each sample.

B. Two-fluid model

The two-fluid model is often used to describe the electrodynamics of a homogeneous, isotropic superconductor below the gap frequency.[47] Some temperature-dependent fraction n_s/n of the electrons is in the condensed phase or superconducting state, while the remainder n_n/n are in the excited or normal state. In the implementation of the two-fluid model used here, the fraction of normal electrons, n_n/n, is assumed not to have the usual temperature dependence, but is used as a free parameter. The conductivity can be written as

$$\sigma(\omega)=\frac{\sigma_0}{1-i\omega\tau}+i\frac{c^2}{4\pi\lambda_{\rm tf}^2\omega} . \tag{2}$$

The complex normal (quasiparticle) conductivity is written in terms of $\sigma_0=\sigma_{\rm dc}(n_n/n)$, where $\sigma_{\rm dc}=ne^2\tau/m$ is the normal-state conductivity and τ is the momentum-relaxation time. The complex superconducting (pair) conductivity is given in terms of the superconducting penetration depth $\lambda_{\rm tf}$, where

$$\frac{1}{\lambda_{\rm tf}^2}=\frac{4\pi}{c^2}\frac{n_s e^2}{m} .$$

Here m and e are the mass and charge, respectively, of the paired carriers.

We can describe the two-fluid model in terms of an equivalent circuit with frequency-independent lumped circuit elements, as shown in Fig. 7(a). The normal carrier inductivity is $\mathcal{L}_n=m/n_n e^2=\tau/\sigma_0$, and the superconducting carrier inductivity is $\mathcal{L}_s=m/n_s e^2=4\pi\lambda_{\rm tf}^2/c^2$. The inductance per square of a film is equal to the inductivity divided by the film thickness. The free parameters for this model are $\lambda_{\rm tf}$, σ_0, and τ.

At low frequencies for which $\mathcal{L}_n,\mathcal{L}_s \ll 1/\omega\sigma_0$, the penetration of the rf fields is limited by the superconducting electrons, and the absorptivity $A(\omega)=\beta_l\omega^2$, where

$$\beta_l=\sigma_0\mathcal{L}_s^{3/2}/\pi^{1/2}=8\pi\sigma_0\lambda_{\rm tf}^3/c^3 .$$

At intermediate frequencies for which $\mathcal{L}_s \gg 1/\omega\sigma_0 \gg \mathcal{L}_n$, the penetration is limited by the normal electrons, and the absorptivity $A(\omega)\propto\omega^{1/2}$. Above the relaxation frequency of the normal electrons $\mathcal{L}_n\mathcal{L}_s \gg 1/\omega\sigma_0$ and the absorptivity $A(\omega)=\beta_h$, where

$$\beta_h=\mathcal{L}_s^{3/2}/\sigma_0\pi^{1/2}(\mathcal{L}_s+\mathcal{L}_n)^{3/2}\mathcal{L}_n^{1/2}$$

is a constant up to the plasma frequency which is outside of our range. For nonvanishing $\tau=\sigma_0\mathcal{L}_n$, however, the intermediate-frequency limit is accessible only for $n_n > n_s$. Our data do not show a distinct region in which the absorptivity varies as $\omega^{1/2}$.

C. Weakly coupled grain model

Hylton *et al.*[45] proposed a model that treats polycrystalline high-T_c films as a network of weakly coupled grains, as suggested by the morphology of high-T_c superconducting films. In *c*-axis-oriented YBCO thin films, the current flows in the strongly superconducting *ab* planes, but is impeded by grain boundaries.[48] Hylton *et al.* proposed a phenomenological model that ignores the anisotropy of the electrical conductivity in the *ab* plane and as-

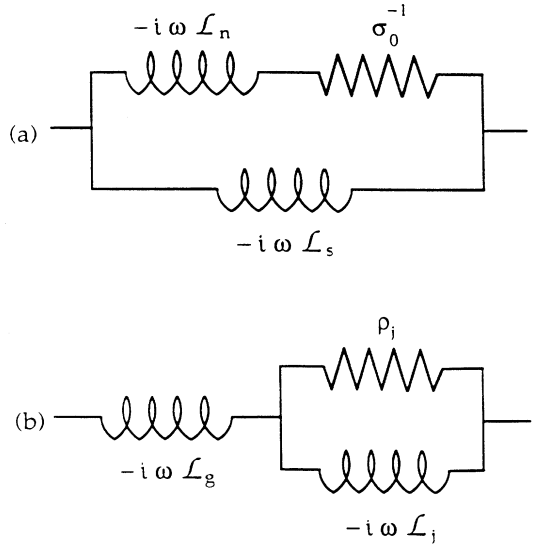

FIG. 7 Equivalent circuits for (a) two-fluid and (b) weakly coupled grain models. A simple circuit transformation shows that these two circuits yield the same form for the frequency-dependent fitting function for the absorptivity. The interpretation of the parameters, however, is different for the two models.

sumes that the material of the grains is an ideal BCS superconductor. The grain boundaries are modeled by resistively shunted Josephson junctions. The distributions of grain size and coupling strength between the grains are then reduced to an effective grain size and coupling strength. It is assumed that the rf current density through the junction is small compared with the critical current I_c of the junction so that the Josephson junction can be approximated as an inductor $L_j=\hbar/2eI_c$. Introducing a characteristic length associated with the average grain size a, the conductivity can be written as

$$\sigma(\omega)^{-1}=-i\omega\mathcal{L}_g+\left[\frac{1}{\rho_j}+\frac{1}{-i\omega\mathcal{L}_j}\right]^{-1}, \tag{3}$$

where the superconducting inductivity of the grains is $\mathcal{L}_g=4\pi\lambda_g^2/c^2$ and the inductivity of the Josephson junction is $\mathcal{L}_j=\hbar/2ej_ca=4\pi\lambda_j^2/c^2$. We obtain a shunt resistivity ρ_j for the junctions by assuming that the grains have characteristic length a. The parameter j_c is the critical-current density of the grain-boundary junction, λ_g is the penetration depth within the grains, and λ_j is the Josephson penetration depth of the junction. The equivalent circuit that represents this response is shown in Fig. 7(b). The effective superconducting penetration depth λ_{eff} that would be measured in a magnetic-field-penetration experiment[46] is given by

$$\lambda_{\text{eff}}^2=\lambda_g^2+\lambda_j^2 . \tag{4}$$

This parameter includes the effects of both the superconducting grains and the Josephson coupling between the grains.

The functional form for $\sigma(\omega)$ in the two-fluid model is identical to that in the weakly coupled grain model. Expressing the parameters of the two-fluid model in terms of the weakly coupled grain-model parameters, we find

$$\mathcal{L}_s=\mathcal{L}_g+\mathcal{L}_j , \tag{5a}$$

$$\mathcal{L}_n=\left[\frac{\mathcal{L}_g}{\mathcal{L}_j}\right](\mathcal{L}_g+\mathcal{L}_j) , \tag{5b}$$

$$\sigma_0^{-1}=\rho_j\left[\frac{\mathcal{L}_g+\mathcal{L}_j}{\mathcal{L}_j}\right]^2 . \tag{5c}$$

Equation (5a) is equivalent to eq. (4) and shows that λ_{tf} in the two-fluid model is equal to λ_{eff} in the weakly coupled grain model.

D. Model fitting

The two phenomenological models described above yield a single, three-parameter frequency-dependent conductivity $\sigma(\omega)$. The parameters can be interpreted either in terms of the two-fluid or weakly coupled grain model. The three-parameter conductivity $\sigma(\omega)$ is used to calculate the absorptivity $A(\omega)$ from

$$A(\omega)=1-\left|\frac{4\pi/c-Z(\omega)}{4\pi/c+Z(\omega)}\right|^2 , \tag{6}$$

where

$$Z(\omega)=(4\pi/c)[\varepsilon_\infty+i4\pi\sigma(\omega)/\omega]^{-1/2} ,$$

and where the film is assumed to be much thicker than the penetration depth. The value of ε_∞ includes the effects of absorption above $\sim 1000\ \text{cm}^{-1}$. We find that for $\varepsilon_\infty<20$ the precise value of ε_∞ has no effect on the data analysis below $\sim 700\ \text{cm}^{-1}$. As a consequence, the fitting function $A(\omega)$ contains just three independent parameters.

The three-parameter fitting function was fit to the absorptivity spectra by a χ^2 minimization. A subset of 20 submillimeter points along with the microwave data point was used in the fitting for each sample. The data from the submillimeter spectral range were chosen to lie between ~ 40 and $400\ \text{cm}^{-1}$ to avoid the onset of additional absorptivity above $450\ \text{cm}^{-1}$ and were uniformly spaced in $\log_{10}$[frequency] so as not to overemphasize higher-frequency data. When features such as the optical phonon at $150\ \text{cm}^{-1}$ are avoided, the absorptivity spectra are smooth and the precise values of the chosen frequencies are unimportant. The statistical uncertainty used in fitting the data was arbitrarily set equal to 15% of the loss measured at each frequency. The three-parameter fitting function can be made to agree quite well with the data. However, since the data below the absorption edge at $450\ \text{cm}^{-1}$ do not contain enough information to determine uniquely all three independent parameters, fits can be obtained for a range of parameter values. We use the penetration depth of 140 nm obtained from μsr experiments[49] to constrain the models in two different ways.

Our use of the μsr data to constrain the weakly coupled grain model is complicated by the interpretation of the μsr data for inhomogeneous materials. The magnetic distribution within the bulk of the material, i.e., the grains, can be approximated by a perfect vortex lattice. Defects at inhomogeneities such as grain and twin boundaries, however, tend to pin the magnetic vortices, which then increase the field variation.[50] In principle, the μsr experiment measures the volume-weighted distribution of magnetic fields throughout the sample. In practice, there is a tendency to focus on the rather narrow distribution of fields in the grains which comprise most of the sample volume rather than the broader distribution of fields in the grain or twin boundaries which comprise a much smaller volume. To the extent that this is the case, the μsr experiment measures λ_g, and not λ_{eff}.

The fits to the absorptivity data with $\lambda_g=140$ nm are called fit I and are shown in Fig. 6 as long-dashed lines. Good fits are obtained to the submillimeter data and the microwave R_s for all five films measured. Results of this analysis are listed in Table III. Uncertainties for each sample in Table III are estimated from constant χ^2 boundaries which define an arbitrary confidence region about the best fit. Errors indicate relative uncertainties between the parameters and do not include any uncertainty in λ_g. Any analysis of submillimeter data using the weakly coupled grain model suffers from the problem that most of the discussions in the literature use two-fluid concepts which are only appropriate for a homogeneous material. In order to make contact with this literature, we convert

TABLE III. Model parameters deduced from fit I to the measured absorptivity. This fit is successful for all films measured. The weakly coupled grain-model parameters correspond to the assumption that $\lambda_g = 140$ nm, which is physically reasonable for all films. Values of λ_{tf} deduced from this fit range from 200 nm in our films with lowest absorptivity to 520 in our highest-loss film.

Sample	λ_j (nm)	ρ_j ($\mu\Omega$ cm)	I_cR (mV)	a[a] (nm)	$\lambda_{eff}=\lambda_{tf}$ (nm)	σ_0 [$\times 10^3$ (Ω cm)$^{-1}$]	$\hbar/\tau$[b] (cm^{-1})	l[c] (nm)	n_n/n (%)	ω_{p0} (eV)
A	148±17	93 ±25	11.0±2.5	40±10	204±12	3.0±0.5	377±80	3.1±0.6	53±33	1.4±0.2
B	175±30	57±18	4.9±1.2	29±12	224±23	6.5±1.5	201±50	5.8±1.4	61±52	1.4±0.3
C	265±55	216±90	8.0±2.1	12±5	299±49	2.8±0.9	596±196	2.0±0.6	78±96	1.4±0.4
D	160±20	41±9	4.2±0.9	34±10	212±15	7.8±1.6	157±31	7.4±1.5	57±39	1.4±0.2
E	502±100	300±150	3.1±0.6	4±1	521±96	2.8±1.0	702±256	1.7±0.6	93±131	1.4±0.5

[a]Values of the effective grain length a calculated assuming $j_c = 3\times 10^7$ A cm^{-2}.
[b]The scattering rate $\hbar/\tau$ in wave numbers is given by $(2\pi c\tau)^{-1}$.
[c]Values of the electronic mean free path l are calculated assuming $v_F = 2.2\times 10^7$ cm s^{-1}.

the weakly coupled grain-model parameters obtained by setting $\lambda_g = 140$ nm to the two-fluid model parameters σ_0, $\hbar/\tau$, and $\lambda_{tf}=\lambda_{eff}$, which give the same excellent fit I to the absorptivity. The values of both the two-fluid and the weakly coupled grain parameters obtained in this way are listed in Table III.

The two-fluid parameters in Table III correspond to values of λ_{tf} which vary from 200 nm in the films with the lowest absorptivity to 520 nm in the film with the highest absorptivity. These values are in fact consistent with the results for the magnetic-field-penetration depth from microstrip resonator experiments[51] on films. Since the penetration depth in films may actually be larger than for single crystals, it can be argued that the two-fluid parameters for fit I in Table III have physical meaning.

An alternative way to constrain the two-fluid model is to use the μsr result and set $\lambda_{tf}=140$ nm. The results of this procedure, called fit II, are shown in Fig. 6 as the short-dashed lines. A good fit to the measured absorptivity is found for the low-absorptivity samples A, B, and D, which smoothly joins the submillimeter data to the microwave R_s. However, fit II is not successful for the higher-loss samples C and E, which are expected to have larger penetration depths. In the case of film E, which has high residual loss, the fit does not even intersect the data. The fit can be forced to intersect the data, but the resulting slope at high frequencies is then so small that the value of χ^2 is increased. Results of this analysis are shown in Table IV for the low-loss samples. The discrepancy between the two sets of parameters for films A, B, and D can be interpreted as a measure of our ignorance of the proper physical constraint for the two-fluid model fit.

We can understand the poor quality of fit II for the high-absorptivity films C and E in the following way. If the two-fluid model with $\lambda_{tf}=140$ nm adequately describes the losses in low-absorptivity films, then as film quality decreases, perhaps as a result of increased granularity, the absorptivity of the films increases, and we expect that the superconducting penetration depth λ_{tf} will increase. By fixing λ_{tf} we ensure that our simple model given by fit II will not be able to describe the optical properties of the high-absorptivity films.

E. Discussion of fits

1. *Scattering rate*

Reflectivity measurements made on YBCO thin films at temperatures just above $T_c \sim 90$ K obtain values of $\hbar/\tau \sim 100$ cm^{-1}. Assuming a BCS gap of $3.5k_BT_c$, this result implies that YBCO is in the clean limit of the classical skin-effect regime of superconductivity ($\hbar/\tau \ll 2\Delta, \xi_0 \ll l \ll \lambda_L$).[2] It is reasonable to assume that the quasiparticle-scattering rate should rapidly decrease for temperatures below T_c. Such behavior has been observed by several groups.[12,52,53] However, at low temperature we find scattering rates of 150 cm$^{-1} > \hbar/\tau > 700$ cm^{-1} for all films measured, corresponding to values of the electronic mean free path l between 2 and 7 nm, assuming $v_F = 2.2\times 10^7$ cm s^{-1}.[14] It is interesting to speculate on possible explanations for a faster scattering at low temperatures, which is a property of both the parameters of Tables III and IV.

TABLE IV. Two-fluid model parameters deduced from fit II, which is successful only for the highest-quality films A, B, and D. From the two-fluid viewpoint, this fit corresponds to setting λ_{tf} equal to the μsr result of 140 nm. This fit can also be obtained from a weakly coupled grain-model viewpoint, but only with the nonphysical constraint that $\lambda_{eff}=140$ nm.

Sample	σ_0 [$\times 10^3$ (Ω cm)$^{-1}$]	$\hbar/\tau$ (cm^{-1})	l[a] (nm)	n_n/n (%)	ω_{p0} (eV)
A	12±3	566±210	2.0±0.8	75±77	2.9±0.6
B	28±8	426±215	2.7±1.4	85±123	3.6±1.2
D	36±16	305±195	3.8±2.4	84±165	3.5±1.6

[a]Values of the electronic mean free path l calculated assuming $v_F = 2.2\times 10^7$ cm s^{-1}.

A scattering rate $\hbar/\tau$ which is larger in the superconducting state than above T_c can be understood if we postulate that the film contains two types of carriers, which we call "condensing electrons" and "noncondensing electrons." The condensing electron condense rapidly into the superconducting ground state below T_c as in a BCS superconductor. The noncondensing electrons remain in the normal state at all temperatures. If the condensing electrons have a slow scattering rate and a large oscillator strength and the noncondensing electrons have a fast scattering rate and a relatively small oscillator strength, then the effective conductivity of the composite system above T_c will be dominated by the condensing electrons. Below T_c where the condensing electrons have all condensed, the scattering will be dominated by the noncondensing electrons and a faster scattering rate will be measured.

2. Superconducting penetration depth

We can determine the superconducting penetration depth from infrared measurements by determining the "missing area" between $\sigma_1(\omega)=\mathrm{Re}[\sigma(\omega)]$ in the normal and superconducting states. This missing area is the oscillator strength which condenses into a δ function at zero frequency upon entering the superconducting state and is related to the number of condensed carriers and thus to the superconducting penetration depth.[54] Missing-area calculations based on reflectivity measurements using single crystals obtain values for the penetration depth which are consistent with the μsr result of 140 nm,[3,4] not with λ_{eff}, which is larger than 140 nm, as might be expected from the weakly coupled grain model. Differences between the losses in thin films and crystals may account for some of this discrepancy despite the fact that above 400 cm^{-1} the loss in films A, B, and D are nearly identical to the losses in YBCO single crystals with $T_c \sim 90$ K.[3,4] Another possible explanation is a difference between the absorptivity assumed in interpreting the two experiments. In the missing-area calculations, the superconducting-state conductivity $\sigma_1(\omega)$ below 140 cm^{-1} was taken to be either zero[3] or constant[4] and equal to ~ 1400 $(\Omega\ \mathrm{cm})^{-1}$. As discussed in Sec. VI G, we find a larger oscillator strength below 140 cm^{-1} both from fit I and from the KK analysis of our loss data. Inclusion of this additional low-frequency oscillator strength into the missing-area calculation for the superconducting penetration depth λ would lead to larger values of λ. However, λ only increases inversely as the square root of the area difference so that λ is still smaller than λ_{eff}. A third possible explanation is that grain models can be expected to fail at high enough frequencies that the coherence length of the radiation becomes small compared with typical grain sizes.

3. Carrier densities

The normal and superconducting carrier densities n_n and n_s are determined from σ_0/τ and $c^2/(4\pi\lambda_{\mathrm{eff}}^2)$, respectively, using parameters obtained from our modeling. Values for n_n/n determined from Table III (fit I) range from 50% to 60% at 2 K for the low-absorptivity films A, B, and D and from 80% to 90% for the higher-absorptivity films C and E, more than five orders of magnitude larger than the prediction of the Gorter-Casimir two-fluid model, where $n_n/n=(T/T_c)^4$. The values for the low-loss films are consistent with the results of Gao *et al.*,[12] who use a two-fluid model to fit their combined transmissivity and reflectivity data, obtaining values of n_n/n at low temperature between 10% and 50%. Values for n_n/n determined from Table IV (fit II) range from 75% to 85%, where the results are listed only for the low-absorptivity films A, B, and D, which are consistent with the losses described by fit II, as discussed in Sec. VI D.

We can also determine the plasma frequency $\omega_{p0}^2=4\pi(n_n+n_s)(e^2/m)$, which corresponds to the carrier concentration (n_n+n_s). Because our simple models are used to fit the data below the sharp onset at 450 cm^{-1}, ω_{p0} does not contain information about the oscillator strength at frequencies above 450 cm^{-1}. Values for ω_{p0} listed in Table III for fit I are equal to 1.4 eV. Several groups have modeled their low-frequency spectra with a Drude oscillator in an attempt to deduce a temperature-independent plasma frequency corresponding to the free carriers. Our values for ω_{p0} listed in Table III are in good agreement with these optically determined estimates for the Drude plasma frequency, which vary from 1.0 to 1.5 eV.[2,3,12] In contrast, values for ω_{p0} from fit II are larger than or equal to the value of the optically determined plasma frequency $\omega_p=3$ eV corresponding to the total oscillator strength.[14] Since ω_{p0} is determined only from the oscillator strength below ~ 450 cm^{-1}, it must be significantly less than ω_p. This discrepancy, in addition to the results from the Kramers-Kronig analysis presented in Sec. VI G, gives strong evidence that fit II is fundamentally unsatisfactory, despite the fact that it can describe the losses in the lowest-absorptivity films A, B, and D.

4. Weakly coupled grain-model parameters

For the weakly coupled grain model, we have determined the $I_cR=\rho_j j_c a$ product and the characteristic grain length a of the junction. In order to determine a, we must assume a value for the critical-current density j_c, since only the product $j_c a$ is determined from the weakly coupled grain model. We assume that the critical-current density j_c of the grain boundaries is essentially the critical-current density 3×10^7 A cm^{-2} of the films, which is a typical value for high-quality c-axis films at 4 K,[36] in agreement with measurements made on films A and B.[36,37] I_cR products in Table III are consistent with measurements on isolated grain-boundary junctions, which range between 0.2 and 8 mV at 4.2 K.[48] Characteristic grain lengths a range from 4 to 40 nm for all films. These values are roughly consistent with the spatial correlation range in the laser-ablated films of ~ 10 nm (Ref. 33) and with twin domain sizes in off-axis sputtered films of ~ 20–200 nm.[36]

Although the weakly coupled grain model is able to fit our loss data so well, values of a found from the best fits

are considerably smaller than the size of typical 45°-misoriented grains, which range from 0.5 to 10.0 μm.[36] Such high-angle grain boundaries are known to behave as resistively shunted junctions,[48] which could therefore justify the use of the weakly coupled grain model. However, the volume fraction of such grains in our films is typically less than 1%,[36,37] which is an indication that the high-angle grain-boundary junctions probably do not provide the dominant intergrain coupling mechanism in these films. The parameter values deduced from fitting the weakly coupled grain model, however, are quite reasonable considering the simplicity of the model.

F. Including oscillator strength above 450 cm^{-1}

The technique we have used to fit our data explicitly assumes that the absorption mechanism above 450 cm^{-1} does not contribute any oscillator strength below that frequency. This assumption is justified by the sharpness of the onset as seen in Fig. 6. In order to test the sensitivity of the weakly coupled grain and two-fluid model parameters to this assumption, we have analyzed our data including the oscillator strength peaked at $\sim$1000 cm^{-1} proposed by other investigators.[2,15] While the addition of this high-frequency oscillator strength reduces the oscillator strength at the lower frequencies required to fit the data, the effect is quantitatively small and the model parameters obtained in this way are all within the experimental uncertainties reported in Tables III and IV.

G. Kramers-Kronig analysis

As an alternative to the model fitting described above, we have also used the KK-transform technique to deduce the frequency-dependent conductivity $\sigma(\omega)$ from our loss data. In contrast to the fitting procedure, the KK technique requires a knowledge of the loss, or equivalently the reflectivity, for all frequencies. In all practical cases, the loss is measured over some finite frequency interval and extended to zero and infinite frequencies, respectively, by suitable extrapolations. Care must be taken in extending the loss data as considerable uncertainties in the inferred conductivity may result, even at frequencies far from the range of the extrapolations.

We extend our absorptivity data to higher frequencies in two different ways. We have smoothly grafted our data, which ends at 700 cm^{-1}, onto reflectivity data for a similar sample[55] which extends to 5 eV. This reflectivity is roughly constant, with $R\sim0.08$, near 5 eV. We then extrapolate the data to infinite frequency by assuming that the reflectivity remains constant above 5 eV. We have also grafted our loss data onto the data of Tajima *et al.*,[56] which extends to 35 eV. Above this frequency we have extrapolated the reflectivity measured by Tajima *et al.* by an ω^{-4} dependence, which is the free-electron asymptotic limit. Despite the difference between these extrapolations, the conductivities determined by the KK transform for both of these high-frequency extrapolations are nearly identical below 2000 cm^{-1}. The contributions to the low-frequency conductivity from both high-frequency reflectivity extrapolations are consistent. In addition, the conductivity below $\sim$600 cm^{-1} is independent of the precise way in which the sets of measured data are grafted together.

We extend our data to zero frequency by assuming that the loss varies as ω^2 below $\sim$30 cm^{-1}. Within experimental uncertainty this extrapolation intersects the measured microwave loss R_s for all films, as seen in Fig. 6.

The results of this analysis are shown in Fig. 8, where we plot $\sigma_1(\omega)=\mathrm{Re}[\sigma(\omega)]$ for sample B. The solid line is obtained from the KK transform, the long-dashed line is from fit I, and the short-dashed line is from fit II. This figure is representative of the results obtained for all samples. We find remarkable agreement between the conductivity determined from the KK transform and that from fit I. This agreement supports the parameter set obtained from the weakly coupled grain model by setting $\lambda_g=140$ nm as a phenomenological description of the submillimeter and millimeter wave losses in YBCO. In particular, this agreement gives us confidence in our interpretation of λ_g, not λ_{eff}, as the superconducting penetration depth which is analogous to the penetration depth measured by μsr techniques, as discussed in Secs. VI C and VI D. The two-fluid model is also successful if the values of λ_{tf} in Table III are used to constrain the fit. If, however, we choose $\lambda_{\mathrm{tf}}=140$ nm in the two-fluid model, the conductivities resulting from the best fit of the model to the absorptivity data are consistently larger than the results of the KK analysis for frequencies below 700 cm^{-1}.

The results for $\sigma_1(\omega)$ from the KK transform are in agreement with those from other workers, both in magnitude and overall shape for frequencies above $\sim$400 cm^{-1}.[2-7] In particular, we observe the well-known conductivity onset at 450 cm^{-1}. Below 400 cm^{-1} we observe that the conductivity rises slowly to a maximum at $\omega=0$ with values of $\sigma_1(0)$ ranging from 3000 to 8000 $(\Omega\,\mathrm{cm})^{-1}$ for all samples. This result is consistent with two recent reflectivity experiments,[5,6] one of which was extended with a measurement of the microwave loss at 87 GHz.[6]

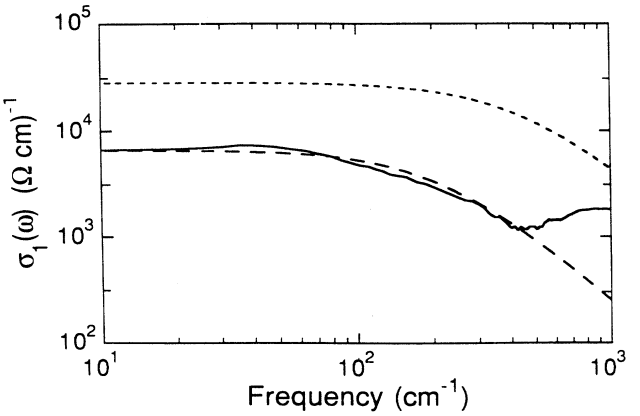

FIG. 8. Values of $\sigma_1(\omega)$ for sample B determined from a Kramers-Kronig analysis (solid line), from the best fit of either the two-fluid model with $\lambda_{\mathrm{tf}}=140$ nm or the weakly coupled grain model with $\lambda_{\mathrm{eff}}=140$ nm (short-dashed line) and from the best fit of the weakly coupled grain model with $\lambda_g=140$ nm (long-dashed line).

It is interesting to note that our results are also consistent above ~ 100 cm^{-1} with the a-axis conductivity determined from the directly measured absorptivity of a detwinned single crystal of $YBa_2Cu_3O_7$.[11] However, below 400 cm^{-1} our results are in disagreement with the low-temperature, low-frequency conductivity determined from KK transforms of reflectivity data,[2,3,7] from a combined transmissivity and reflectivity measurement,[12] and from another direct absorptivity measurement on single crystals.[21] Possible sources for this discrepancy will be discussed in a future publication.[57]

VII. CONCLUSIONS

We have measured the residual loss in six ab-plane epitaxial thin films of $YBa_2Cu_3O_7$ from 30 cm^{-1} (1.5 THz) to 700 cm^{-1} (21 THz) and for five of the six films near 0.3 cm^{-1} (10 GHz). We do not observe any gaplike features below 450 cm^{-1}, nor is there any indication of an onset of absorptivity at ~ 140 cm^{-1}. For each of the five films, the loss measured near 0.3 cm^{-1} can be connected to the submillimeter data at ~ 30 cm^{-1} by a line which varies as the frequency squared. Above ~ 30 cm^{-1} the loss saturates smoothly in a way which is different for different films. Above 450 cm^{-1} there is a sudden onset of additional absorptivity and the loss data diverge rapidly from model fits, suggesting the onset of an additional absorption mechanism.

We have used both a homogeneous two-fluid model and an inhomogeneous weakly coupled grain model for the electrical conductivity to fit the frequency-dependent absorptivity below the onset at 450 cm^{-1}. Both of these models yield the same three-parameter fitting function. Because our models are strictly valid at frequencies below the superconducting gap, our model fitting implicitly assumes that the superconducting energy gap 2Δ, if one exists, occurs at or above 450 cm^{-1}. We find that the inhomogeneous weakly coupled grain model is able to smoothly fit the data for all films (fit I) from 0.3 cm^{-1} (10 GHz) to 450 cm^{-1} (13.5 THz) when the parameter λ_g corresponding to the superconducting penetration depth within the BCS-like grains is constrained by the μsr result. Our use of the μsr data to constrain λ_g in the weakly coupled grain model is consistent with the interpretation of the μsr measurement for inhomogeneous materials.[50]

Fit I is also equivalent to a two-fluid model in which λ_{tf} varies from ~ 1.5 times the μsr result for our lowest-absorptivity films to ~ 3.7 times the μsr result for our highest-absorptivity film. The total carrier density $(n_n + n_s)$ determined from this two-fluid interpretation of fit I is in agreement with optically determined estimates for the free-carrier oscillator strength, and the conductivity determined from fit I is in excellent agreement with a KK analysis of the absorptivity data. However, when λ_{tf} is constrained by the μsr result to 140 nm, the resulting fit II is only satisfactory for our lowest-absorptivity films. In addition, the results are not consistent with the optically determined plasma frequency or the KK conductivity. Both fits correspond to a relaxation rate $\hbar/\tau$ for the normal carriers that produce the residual loss that is significantly larger than the rate deduced for $T > T_c$. The fact that the successful fit I comes naturally from a weakly coupled grain model with no adjustable parameters suggests that weak-link behavior may play a significant role in the microwave and submillimeter losses. Values of junction I_cR products and a characteristic length determined from the model best fits are consistent with these independently measured quantities.

ACKNOWLEDGMENTS

We gratefully acknowledge C. A. Mears, T. W. Kenny, R. C. Taber, J. Beeman, J. Emes, E. Haller, A. T. Barfknecht, W. N. Creager, J. R. Waldram, J. Orenstein, and A. E. Zettl for their assistance in various aspects of this work. This work was supported in part by the Director, Office of Energy Research, Office of Basic Energy Sciences, Materials Sciences Division of the U.S. Department of Energy under Contract No. DE-AC03-76SF00098 (D.M. and P.L.R.), by the AFOSR under Contract No. F49620-88-C-004 (C.B.E. and T.H.G.), and by the Center for Research in Superconductivity and Superconducting Electronics under Contract No. F49620-88-C-001 (C.B.E. and T.H.G.).

[1]Z. Schlesinger, R. T. Collins, D. L. Kaiser, and F. Holtzberg, Phys. Rev. Lett. **59**, 1958 (1987).

[2]K. Kamaras, L. L. Herr, C. D. Porter, N. Tache, D. B. Tanner, S. Etemad, T. Venkatesan, E. Chase, A. Inam, X. D. Wu, M. S. Hegde, and B. Dutta, Phys. Rev. Lett. **64**, 84 (1990).

[3]J. Orenstein, G. A. Thomas, A. J. Millis, S. L. Cooper, D. H. Rapkine, T. Timusk, L. F. Schneemeyer, and J. V. Waszczak, Phys. Rev. B **42**, 6342 (1990).

[4]Z. Schlesinger, R. T. Collins, F. Holtzberg, C. Field, G. Koren, and A. Gupta, Phys. Rev. B **41**, 11 237 (1990).

[5]D. vanderMarel, M. Bauer, E. H. Brandt, H. U. Habermeier, D. Heitmann, W. Konig, and A. Wittlin, Phys. Rev. B **43**, 8606 (1991).

[6]K. F. Renk, B. Gorshunov, J. Schutzmann, A. Pruckl, B. Brunner, J. Betz, S. Orbach, N. Klein, G. Muller, and H. Piel, Europhys. Lett. **15**, 661 (1991).

[7]J. Schutzmann, W. Ose, J. Keller, K. F. Renk, B. Roas, L. Schultz, and G. Saemann-Ischenko, Europhys. Lett. **8**, 679 (1989).

[8]R. T. Collins, Z. Schlesinger, R. H. Koch, R. B. Laibowitz, T. S. Plaskett, P. Freitas, W. J. Gallagher, R. L. Sandstrom, and T. R. Dinger, Phys. Rev. Lett. **59**, 704 (1987).

[9]G. A. Thomas, J. Orenstein, D. H. Rapkine, M. Capizzi, A. J. Millis, R. N. Bhatt, L. F. Schneemeyer, and J. V. Waszczak, Phys. Rev. Lett. **61**, 1313 (1988).

[10]Z. Schlesinger, R. T. Collins, F. Holtzberg, C. Feild, S. H. Blanton, U. Welp, G. W. Crabtree, Y. Fang, and J. Z. Liu, Phys. Rev. Lett. **65**, 801 (1990).

[11]T. Pham, M. W. Lee, H. D. Drew, U. Welp, and Y. Fang, Phys. Rev. B **44**, 5377 (1991).

[12]F. Gao, G. L. Carr, Porter, D. B. Tanner, S. Etemad, T. Venkatesan, A. Inam, B. Dutta, X. D. Wu, G. P. Williams, and C. J. Hirschmugl, Phys. Rev. B **43**, 10 383 (1991).

[13]G. P. Williams, R. C. Budhani, C. J. Hirschmugl, G. L. Carr,

S. Perkowitz, B. Lou, and T. R. Yang, Phys. Rev. B **41**, 4752 (1990).

[14]B. Batlogg, in *High Temperature Superconductivity Proceedings, Los Alamos Symposium 1989,* edited by K. S. Bedell, D. Coffey, D. E. Meltzer, D. Pines, and J. R. Schrieffer (Addision-Wesley, Redwood City, CA, 1990), p. 37.

[15]T. Timusk and D. B. Tanner, in *Physical Properties of High Temperature Superconductors I,* edited by D. M. Ginsberg (World Scientific, Teaneck, NJ, 1989), p. 339.

[16]T. Timusk, C. D. Porter, and D. B. Tanner, Phys. Rev. Lett. **66**, 663 (1991).

[17]D. C. Mattis and J. Bardeen, Phys. Rev. **111**, 412 (1958).

[18]H. Piel and G. Muller, IEEE Trans. Magn. **MAG-27**, 854 (1991).

[19]D. Miller, P. L. Richards, S. Etemad, A. Inam, T. Venkatesan, B. Dutta, X. D. Wu, C. B. Eom, T. H. Gegalle, N. Newman, and B. F. Cole, Appl. Phys. Lett. **59**, 2326 (1991).

[20]D. Miller, T. W. Kenny, P. L. Richards, S. R. Spielman, and T. H. Geballe, Bull. Am. Phys. Soc. **34**, 792 (1989).

[21]T. Pham, H. D. Drew, S. H. Moseley, and J. Z. Liu, Phys. Rev. B **41**, 11 681 (1990).

[22]K. F. Renk, J. Schutzmann, A. Pruckl, B. Roas, L. Schultz, and G. Saemann-Ischenko, Physica B **165&166**, 1253 (1990).

[23]N. S. Nishoka, P. L. Richards, and D. P. Woody, Appl. Opt. **17**, 1562 (1978).

[24]E. E. Haller, Infrared Phys. **25**, 257 (1985).

[25]NiCr resistors are manufactored by Mini-Systems Inc., North Attleboro, MA 02761.

[26]The infrared absorber is made from precast Eccosorb CR110, Emerson and Cuming, Gardena, CA.

[27]C. Kittel *Introduction to Solid State Physics* (Wiley, New York, 1986).

[28]R. G. Chambers and A. B. Pippard, Inst. Met. Monog. Rep. Ser **13**, 281 (1953).

[29]W. Koster and H. P. Rave, Z. Metallkd. **55**, 750 (1964).

[30]M. Halpern, H. P. Gush, E. Wichnow, and V. deCosmo, Appl. Opt. **25**, 565 (1986).

[31]C. B. Eom, J. Z. Sun, K. Yamamoto, A. F. Marshall, K. E. Luther, and T. H. Geballe, Appl. Phys. Lett. **55**, 595 (1989).

[32]N. Newman, K. Char, S. M. Garrison, R. W. Barton, R. C. Taber, C. B. Eom, T. H. Geballe, and B. Wilkens, Appl. Phys. Lett. **57**, 520 (1990).

[33]A. Inam, M. S. Hegde, X. D. Wu, T. Venkatesan, P. England, P. F. Miceli, E. W. Chase, C. C. Chang, J. M. Tarascon, and J. B. Wachtman, Appl. Phys. Lett. **53**, 908 (1988).

[34]D. M. Hwang, T. Venkatesan, C. C. Chang, L. Nazar, X. D. Wu, A. Inam, and M. S. Hegde, Appl. Phys. Lett. **54**, 1702 (1989).

[35]A. Inam, X. D. Wu, L. Nazar, M. S. Hegde, C. T. Rogers, T. Venkatesan, R. W. Simon, K. Daly, H. Padamsee, J. Kirchgessner, D. Moffat, D. Rubin, Q. S. Shu, D. Kalokitis, A. Fathy, V. Pendrick, R. Brown, B. Brycki, E. Belohoubek, L. Drabeck, G. Gruner, R. Hammond, F. Gamble, B. M. Lairson, and J. C. Bravman, Appl. Phys. Lett. **56**, 1178 (1990).

[36]C. B. Eom, J. Z. Sun, B. M. Lairson, S. K. Streiffer, A. F. Marshall, K. Yamamoto, S. M. Anlage, J. C. Bravman, T. H. Geballe, S. S. Laderman, R. C. Taber, and R. D. Jacowitz, Physica C **171**, 354 (1990).

[37]S. S. Laderman, R. C. Taber, R. D. Jacowitz, J. L. Moll, C. B. Eom, T. L. Hylton, A. F. Marshall, T. H. Geballe, and M. R. Beasley, Phys. Rev. B **43**, 2922 (1991).

[38]N. Newman, B. F. Cole, S. M. Garrison, K. Char, and R. C. Taber, IEEE Trans. Magn. **MAG-27**, 1276 (1991).

[39]T. S. Ravi, D. M. Hwang, R Ramesh, S. W. Chan, L. Nazar, C. Y. Chen, A. Inam, and T. Venkatesan, Phys. Rev. B **42**, 10 141 (1990).

[40]J. Sizemore, R. Barton, A. Marshall, J. C. Bravman, M. Naito, and K. Char, IEEE Trans. Magn. **MAG-25**, 2245 (1989).

[41]R. C. Taber, Rev. Sci. Instrum. **61**, 2200 (1990).

[42]H. Padamsee, J. Kirchgessner, D. Moffat, J. Potts, D. L. Rubin, Q. S. Shu, A. Inam, X. D. Wu, L. Nazar, M. S. Hegde, and T. Venkatesan (unpublished).

[43]N. Klein, H. Chaloupka, G. Muller, S. Orbach, H. Piel, B. Roas, L. Schulz, U. Klein, and M. Peiniger, J. Appl. Phys. **67**, 6940 (1990).

[44]R. Feile, Physica C **159**, 1 (1989).

[45]T. L. Hylton, A. Kapitulnik, M. R. Beasley, J. P. Carini, L. Drabeck, and G. Gruner, Appl. Phys. Lett. **53**, 1343 (1988).

[46]T. L. Hylton and M. R. Beasley, Phys. Rev. B **39**, 9042 (1989).

[47]T. Vanduzer and C. W. Turner, *Principles of Superconducting Devices and Circuits* (Elsevier, New York, 1981).

[48]R. Gross, P. Chaudhari, M. Kawasaki, and A. Gupta, IEEE Trans Magn. **MAG-27**, 3227 (1991).

[49]D. R. Harshman, L. F. Schneemeyer, J. V. Waszczak, G. Aeppli, R. J. Cava, B. Batlogg, L. W. Rupp, E. J. Ansaldo, and D. L. Williams, Phys. Rev. B **39**, 851 (1989).

[50]E. H. Brandt, Phys. Rev. B **37**, 2349 (1988).

[51]S. M. Anlage, H. Sze, H. J. Snortland, S. Tahara, B. Langley, C. B. Eom, M. R. Beasley, and R. Taber, Appl. Phys. Lett. **54**, 2710 (1989).

[52]D. A. Bonn, R. Liang, D. J. Baar, D. C. Morgan, P. Dosanjh, W. N. Hardy, C. Kallin, and A. J. Berlinsky (unpublished).

[53]D. B. Romero, C. D. Porter, D. B.. Tanner, L. Forro, D. Mandrus, L. Mihaly, G. L. Carr, and G. P. Williams, Phys. Rev. Lett. **68**, 1590 (1992).

[54]M. Tinkham, *Introduction to Superconductivity* (McGraw-Hill, New York, 1975).

[55]K. Kamaras and S. Etemad (private communication).

[56]S. Tajima, H. Ishii, T. Nakahashi, T. Takagi, S. Uchida, M. Seki, S. Suga, Y. Hidaka, M. Suzuki, T. Murakami, K. Oka, and H. Unoki, J. Opt. Soc. Am B **6**, 475 (1989).

[57]D. Miller and P. L. Richards, Phys. Rev. B (to be published).